Proceedings of the 11th ICPMG 2026
11th International Conference on Physical Modelling in Geotechnics
8-12 June 2026, Zurich, Switzerland

Development of Numerical Analysis Model for Evaluating the Dynamic Behavior of Excavated Tunnels

D.H. Baek, M.T. Yoo
Gachon University, Seongnam, Republic of Korea, bsa9312@gachon.ac.kr, minteakyoo@gachon.ac.kr

S.J. Kim
Korea Institute of Civil Engineering and Building Technology (KICT), Goyang, Republic of Korea, seokjungkim@kict.re.kr

I.W. Lee, J.J. Park
Korea Railroad Research Institute (KRRI), Uiwang, Republic of Korea, iwlee@krri.re.kr, jjpark@krri.re.kr

ABSTRACT: OpenSees is an open-source finite element analysis program specialized for soil-structureinteraction and seismic dynamic analysis. In this study, a numerical model for an excavated tunnel was developed using OpenSees, and dynamic analyses were conducted under various conditions to evaluate both ground acceleration and tunnel moment responses. The ground conditions were classified according to rock stiffness into hard rock, soft rock, weathered rock, and fault zone. The structure depth was set at 15m, and analyses were performed for a total of four cases. For input ground motions, 20 domestic and international recorded earthquakes were applied, scaled by factors of 1.0, 1.5, and 2.0. The dynamic analysis results indicated that the acceleration response showed an increasing trend as rock stiffness decreased; however, the amplification relative to the input ground motion was minimal. The maximum bending moment response showed a clear increasing trend as stiffness decreased. In particular, within Fault zones characterized by low stiffness, the seismic response moments induced in the tunnel lining exceeded the allowable bending capacity across all three earthquake scenarios. This suggests that, in contrast to the inherent safety typically associated with competent rock masses, Fault zones with significant stiffness contrast trigger stress concentrations that transcend the structural limits of the lining. Consequently, it is imperative to prioritize rigorous geological characterization and site-specific seismic risk assessments that incorporate the unique dynamic properties of these vulnerable geological formations.

1 INTRODUCTION

In recent years, the frequency of moderate-magnitude earthquakes, including the Gyeongju (M_W 5.8, 2016) and Pohang (M_W 5.4, 2017) events, has significantly increased in Korea, highlighting the seismic safety of major social infrastructure as a critical societal concern. Meanwhile, rapid urbanization has intensified land use density, driving a continuous expansion in the development and utilization of underground spaces, such as subways, tunnels, utility corridors, and large-scale underground commercial facilities. As reliance on underground spaces continues to grow amid escalating seismic hazards, understanding and assessing the seismic behavior and safety of underground structures once regarded as relatively safe have become important issues in seismic engineering research.

Early studies in earthquake engineering primarily focused on evaluating the seismic risk of above-ground structures such as buildings and bridges. For example, Kappos et al., (2006) proposed a hybrid analytical method to evaluate the seismic fragility of reinforced concrete and masonry buildings, while Fajfar et al., (2000) developed a nonlinear analysis framework for performance based seismic design of building structures, establishing a foundation for quantitatively assessing structural response and fragility under earthquake loading.

However, with the growing importance of underground spaces in recent years, research has gradually expanded to the seismic stability assessment of underground structures, and corresponding quantitative evaluation studies have been actively conducted. For example, Kwon et al., (2020) performed dynamic numerical analyses on cut-and-cover subway station structures constructed in sandy soils and developed seismic fragility functions, while O'Rourke et al., (1999) analyzed the seismic behavior of buried pipelines. These studies have mainly focused on the behavior of underground structures embedded in soil deposits; however, several studies have also been conducted on the seismic response of tunnel structures. For instance, Argyroudis et al., (2012) proposed seismic fragility functions for shallow box type tunnels.

Conversely, it has been widely perceived that excavated tunnels in rock masses are inherently resilient to seismic loading owing to the substantial confinement effect provided by the surrounding geological environment (Hashash et al., 2001). Consequently, quantitative seismic performance data for such tunnels remains considerably sparse relative to other types of underground infrastructure. However, conventional design practices predicated on the perceived safety of rock tunnels risk underestimating the dynamic response in Fault zones, where rock mass stiffness undergoes significant degradation. Therefore, a rigorous evaluation of low-stiffness rock formations is imperative to ensure structural integrity during seismic events.

To this end, this study develops a dynamic numerical model for excavated tunnels embedded in various rock mass conditions. By comparing the bending moment responses of the lining with its allowable capacities under different seismic scenarios, this research aims to quantitatively evaluate the effects of rock mass stiffness and seismic intensity on the seismic performance and structural safety of excavated tunnels.

2 NUMERICAL ANALYSIS MODEL

2.1 Numerical Model

For the analysis of soil-tunnel interaction and dynamic behavior under seismic loading, this study utilized OpenSees, an open-source computational framework that has been extensively validated in nonlinear earthquake engineering applications.

First, the ground domain was modeled assuming two-dimensional (2D) plane strain conditions, representing a domain 80 m in width and 50 m in height, and was discretized using 4-node plane strain elements. The bottom boundary of the model was assumed to represent the bedrock layer where seismic waves are input.

Finite element numerical analysis in OpenSees inevitably introduces artificial boundaries due to the constraints of a finite computational domain. To mitigate numerical distortion caused by wave reflections at these boundaries, specialized boundary conditions were implemented. Specifically, the lateral boundaries were configured to represent free-field motion, where seismic waves propagate one-dimensionally. To achieve this, the boundaries were positioned at a sufficient distance of 40 m from the tunnel center, ensuring an adequate domain to prevent interference from reflected waves (Hashash et al.,2001). Furthermore, the equalDOF constraint was applied to the lateral boundaries. By coupling the horizontal degrees of freedom (x-DOF) of corresponding nodes at equivalent depths on both sides, the model effectively simulates one-dimensional shear deformation. This approach accurately reproduces the dynamic response of the free-field ground during seismic events

The tunnel structure was modeled as a horseshoe-shaped section with a 10m diameter, embedded at a depth of 15m from the ground surface. It was discretized using 2-node beam-column elements capable of simulating both flexural and axial behavior.

The ground lining interface was modeled using a no-slip condition by coupling the degrees of freedom of corresponding nodes. In numerical modeling, adopting a slip condition typically allows for interface movement and subsequent stress relaxation, which results in reduced internal forces within the lining. In contrast, the no-slip condition prevents such relaxation, leading to the maximization of internal force transfer between the ground and the structure. Therefore, this study intentionally adopted the no-slip assumption as a conservative approach to evaluate the structural response under the most demanding interaction state.

The rock mass was applied using the Drucker-Prager (1952) model, and this model can reflect the pressure-dependent elasto-plastic behavior, which is a key behavioral characteristic of rock mass. The rock mass is modeled using the Drucker-Prager model, with primary input parameters including shear modulus, bulk modulus, cohesion, internal friction angle, density, and dilatation angle. In this study, to analyze the difference in moment response of excavated tunnel structures according to rock conditions, it was classified into four cases according to rock stiffness, and the rock properties for each of the four cases are shown in Table 1. For the classification of the ground and the estimation of physical properties, the RMR classification system by Bieniawski (1989) and the Hoek-Brown failure criterion by Hoek et al. (2002) were mutually applied.

Table 1. Rock Material Properties for Each Case

Input Parameters	Case 1 (Hard rock)	Case 2 (Soft rock)	Case 3 (Weathered rock)	Case 4 (Fault zone)
Young's modulus (GPa)	35	5	2	0.2
Density (ton/m^3)	2.68	2.3	2.2	2.1
Poisson's ratio	0.2	0.28	0.34	0.4
Shear Wave Velocity (m/s)	2300	930	580	260
Internal Friction Angle (°)	45	35	30	25
Cohesion (kPa)	6000	2500	500	100

In dynamic numerical analysis, the mesh size is determined not only by the stress gradient, as in static analysis, but also by the accuracy of seismic wave propagation. This widely accepted criterion in the field of finite element analysis was proposed by Kuhlemeyer and Lysmer (1973). According to their study, to obtain reliable wave propagation results, the maximum element size (l_e) should be sufficiently smaller than the shortest wavelength (λ_{min}) of interest. It is generally recommended that l_e be less than one-eighth of the minimum wavelength, as expressed in Equation (1). The minimum wavelength (λ_{min}) is determined by the minimum shear wave velocity of the ground ($V_{s,min}$) and the maximum effective frequency of the input motion (f_{max}), as shown in Equation (2).

$$l_e \leq \frac{\lambda_{min}}{8} \quad (1)$$

$$\lambda_{min} = \frac{V_{s,min}}{f_{max}} \quad (2)$$

In this analysis, the most conservative condition was adopted by applying the shear wave velocity of the fault-zone ground ($V_{s,min} = 260m/s$) and the maximum effective frequency of the input motion ($f_{max} = 25Hz$). According to Equation (2), the minimum wavelength was calculated as 10.4m = 260/25, and based on Equation (1), the maximum allowable element size was approximately 1.3m = 10.4/8. Therefore, to satisfy the above criteria and ensure the accuracy of the analysis, the mesh size of the ground elements was set to 1.0 m×1.0 m.

The target tunnel was modeled with a horseshoe-shaped cross-section, assuming an excavation width of 10 m to represent the typical dimensions of railway tunnels in Korea. The lining thickness of the tunnel was set to 0.5 m, as shown in Figure 1.

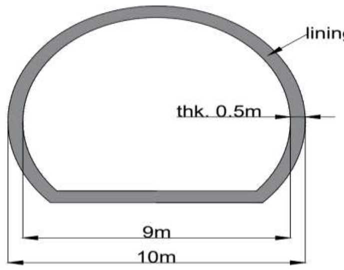

Figure 1. Tunnel Section

The tunnel structure was modeled using the dispBeamColumn element available in OpenSees. This element follows a displacement-based formulation, in which multiple integration points are distributed along the element length to accurately capture the material behavior. It is widely recognized that underground structures exhibit predominantly elastic behavior during earthquakes due to the strong confinement effects of the surrounding ground, particularly in the case of excavated tunnels embedded in rock (Wang et al., 1993). In this analysis, to reflect this characteristic, the cross-section connected to the dispBeamColumn element was defined as section Elastic, assuming linear elastic behavior of the tunnel lining. At this stage, the engineering properties of the tunnel structure were incorporated into the analysis using the section Elastic command, while the lining mass was represented by assigning a specific material density in the definition of the dispBeamColumn element. The input material properties of the excavated tunnel are summarized in Table 2.

Table 2. Input Material Properties of the Tunnel Structure

Young's Modulus (MPa)	Density (ton/m^3)	Element Area (m^2)	Moment of Inertia (m^4)
27,000	2.5	0.5	0.0104

2.2 Input Ground Motion

In this analysis, a total of 20 recorded ground motions were selected as input earthquake excitations. The dataset comprised domestic earthquake records from Gyeongju, Pohang, and Odaesan, which represent the characteristics of the Korean seismic environment, as well as major international ground motions such as the Northridge (1994), Kobe (1995), and Kocaeli (1999) earthquakes, which exhibit long-period and high-energy characteristics. To comprehensively examine the influence of two key parameters rock strength and earthquake intensity on the tunnel bending moment, the selected ground motions were linearly scaled by factors of 1.5 and 2.0 to progressively increase seismic intensity. Accordingly, a total of 60 input ground motions, derived from the combination of 20 earthquake records and three intensity levels, were used to analyze the bending moment response of the tunnel lining under different rock strength conditions.

Prior to the detailed trend analysis, a representative examination of the response characteristics for individual ground motions was conducted. Among the selected input records, the response results for the Kobe 0.62 g (scaled by a factor of 2.0) motion were analyzed and compared across the different cases. The input ground motion had a duration of 30 s and a peak ground acceleration (PGA) of 0.62 g, and its time–acceleration history is shown in Figure 2.

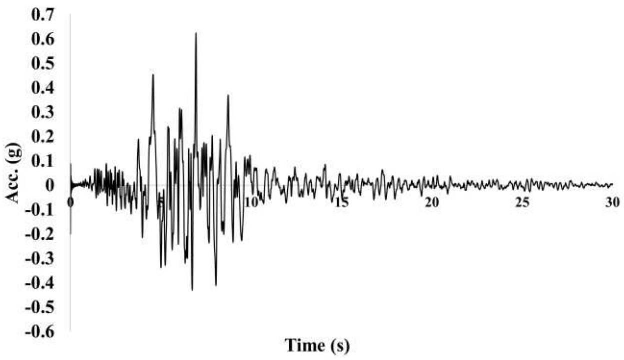

Figure 2. Input Ground Motion (Kobe 0.62g)

3 ANALYSIS RESULTS

3.1 Acceleration Response

Seismic waves originate from the bedrock and propagate upward through the overlying ground layers to the surface, undergoing amplification depending on the inherent dynamic properties of the soil. Accordingly, to analyze the ground amplification characteristics of the acceleration response for each analysis case, the acceleration measurement point was placed at the top of the numerical model. The time–acceleration response histories for each analysis case under the Kobe 0.62g ground motion are shown in Figure 3, and the corresponding peak ground accelerations (PGA) are summarized in Table 3

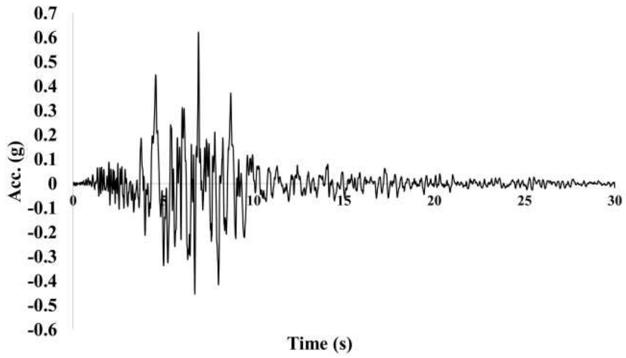

(a) Case-1 (Hard rock)

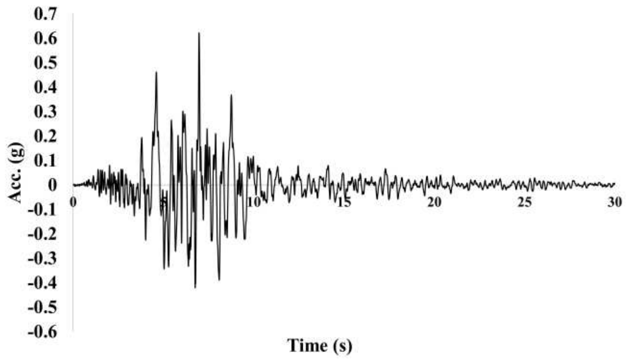

(b) Case-2 (Soft rock)

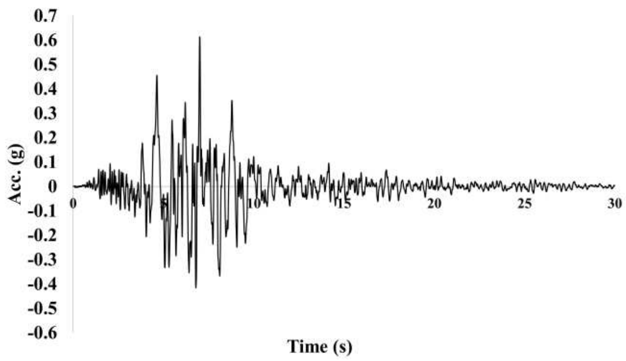

(c) Case-3 (Weathered rock)

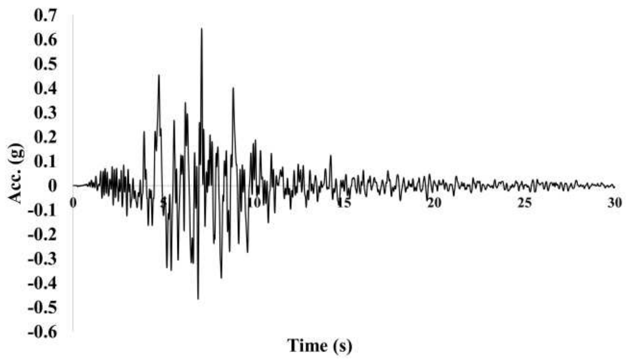

(d) Case-4 (Fault zone)

Figure 3. Acceleration Response by Case

Table 3. Peak Acceleration Response by Case

	Case 1	Case 2	Case 3	Case 4
Input Acceleration (g)	0.624			
Acceleration Response (g)	0.620	0.613	0.615	0.645

As a result of the analysis, no significant amplification of seismic waves was observed under rock conditions ranging from hard rock (Case 1) to weathered rock (Case 3). This behavior can be attributed to the high stiffness of the rock grounds, which was comparable to that of the bedrock, resulting in a minimal impedance contrast between the two media. In general, a larger impedance contrast produces greater ground motion amplification (Kramer, 1996); however, in this case, the small contrast led to negligible amplification. In contrast, the relatively weak fault zone ground (Case 4) exhibited a slight amplification of approximately 4%, owing to the largest impedance contrast with the underlying bedrock among the four cases.

3.2 Bending Moment Response

Before performing a detailed analysis of the moment response trends for each case, the structurally weak zones of the tunnel lining under seismic loading were first identified. To this end, Case 3 (Kobe 0.62g) was selected as the representative case, and the responses at the crown, sidewall, and sidewall–invert junction were compared to determine the location of the maximum bending moment. The results are shown in Table 4.

Table 4. Maximum Bending Moment at Each Measurement Point

Measurement Point	**Crown**	**Sidewall**	**Sidewall-Invert Junction**
Maximum Bending Moment (kN·m)	0.08	1.78	203.02

The bending moment response was greatest at the sidewall–invert junction, where a sharp corner creates a stress concentration point from a structural mechanics perspective. Therefore, the sidewall invert junction identified as the most critical section of the tunnel was selected as the measurement location for comparing the bending moment responses across all analysis cases. The results for each case under the Kobe 0.62g ground motion are summarized in Table 5 and illustrated in Figure 4.

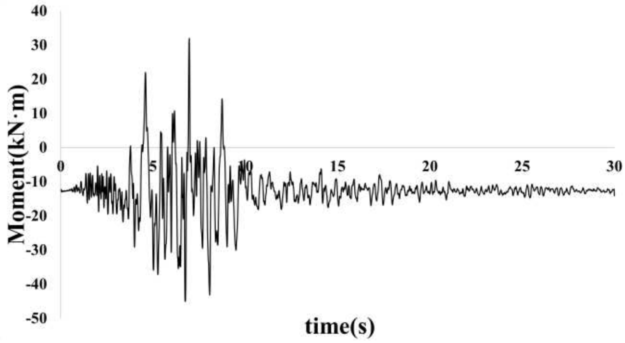

(a) Case-1 (Hard rock)

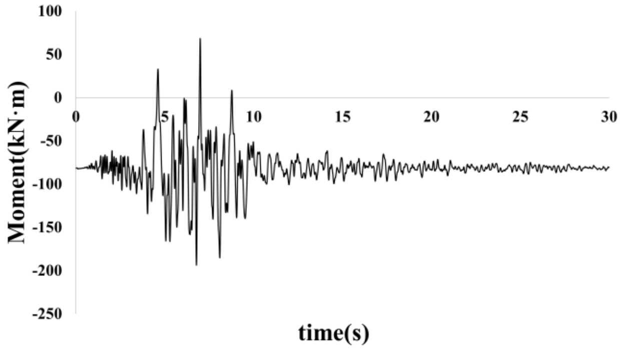

(b) Case-2 (Soft rock)

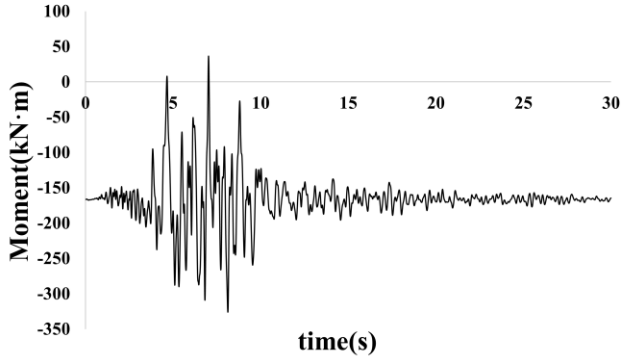

(c) Case-3 (Weathered rock)

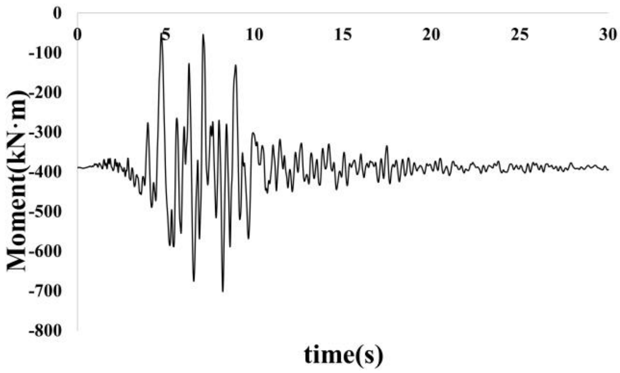

(d) Case-4 (Fault zone)

Figure 4. Moment Response by Case

Table 5. Peak Moment Response by Case

	Case 1	Case 2	Case 3	Case 4
Peak Moment (kN·m)	44.57	149.89	203.02	338.50

The initial moment shown in the graph (at t=0 s) represents the static bending moment in the tunnel lining induced by self-weight. This moment is governed by the stress redistribution that occurs due to soil-structure interaction and the relative stiffness between the ground and the lining. As the rock stiffness decreases, the ground's ability to support its own weight diminishes, resulting in a greater portion of the stress being transferred to the stiffer tunnel lining and, consequently, an increase in the static moment.

In contrast, the dynamic moment generated during seismic loading is primarily controlled by the imposed deformation of the surrounding ground due to seismic wave propagation (Wang et al., 1993). Similar to the static case, this dynamic moment also exhibits an increasing trend as rock stiffness decreases. This is because softer ground experiences larger deformations during shaking, but the relatively stiffer lining resists and cannot fully follow this movement. This incoherence results in greater relative displacement between the ground and the lining, which in turn induces higher bending moments (Hashash et al., 2001).

3.3 Analysis of Maximum Bending Moment Trends Across All Cases

In the previous section, the individual response characteristics under the representative ground motion (Kobe 0.62g) were analyzed. In this section, the scope is expanded to a comprehensive analysis of all 60 cases, combining 20 ground motions with three intensity levels (factors of 1.0, 1.5, and 2.0).

In this study, the allowable bending moment (M_{all}) of the tunnel lining was determined for the quantitative evaluation of dynamic responses in accordance with the Korean Design Standards (KDS 14 20 00 and KDS 47 10 40). Following these standards, the lining section was modeled as a doubly reinforced concrete member (D22@200, SD400) with a width of 1,000 mm and an effective depth of 440 mm. A conservative strength reduction factor ($\emptyset$) of 0.85 was adopted, considering the complex multi-axial stress states of the lining.

As ground stiffness decreases, the soil-structure interaction typically leads to an increase in axial force, which subsequently enhances the flexural capacity of the section. This phenomenon may result in an overestimation of the structural safety margin, particularly in weak ground conditions such as fault zones. To prevent such overestimation, the axial force induced under hard rock conditions where the capacity enhancing effect is minimized was selected as the critical axial force for calculation. Based on this conservative approach, the allowable bending moment was calculated as 587 kN·m, which was established as the failure threshold for evaluating the structural safety of the tunnel lining under seismic loading.

To examine the overall influence of the two key variables, rock strength and seismic intensity, on the lining response and to evaluate the structural safety of the tunnel lining, the maximum bending moment recorded in each case was extracted and plotted together with the allowable bending moment limit. The resulting trend is illustrated in Figure 5.

The findings of this study, which comprehensively analyzed the dynamic behavior of tunnel linings under various rock conditions and seismic intensities based on Figure 5, are summarized as follows.

A consistent trend was observed where the maximum response moments of the lining generally increase as the rock mass stiffness decreases, aligning with established soil-structure interaction theories. As demonstrated in the data distribution of Fig. 5, the entire population of response data exhibits a distinct upward shift toward the allowable bending moment (587 kN·m) as the ground conditions degrade from hard rock to fault zones.

While sound rock and weathered rock conditions mostly maintain stable seismic performance with a sufficient safety buffer, the lower stiffness in fault zones elevates the overall response level, resulting in a relatively higher frequency of scenarios that approach or exceed the allowable limit compared to other ground conditions. This indicates that the structural safety of the tunnel lining is progressively degraded as the ground stiffness decreases. Consequently, these weak ground sections can critically weaken the seismic performance of the tunnel, necessitating prioritized engineering attention and more rigorous evaluations during both the design and construction phases.

The findings of this study, which comprehensively analyzed the dynamic behavior of tunnel linings under various rock conditions and seismic intensities based on Figure 5, are summarized as follows.

A consistent trend was observed where the maximum response moments of the lining generally increase as the rock mass stiffness decreases, aligning with established soil-structure interaction theories. As demonstrated in the data distribution of Fig. 5, the entire population of response data exhibits a distinct upward shift toward the allowable bending moment (587 kN·m) as the ground conditions degrade from hard rock to fault zones.

While sound rock and weathered rock conditions mostly maintain stable seismic performance with a sufficient safety buffer, the lower stiffness in fault zones elevates the overall response level, resulting in

a relatively higher frequency of scenarios that approach or exceed the allowable limit compared to other ground conditions.

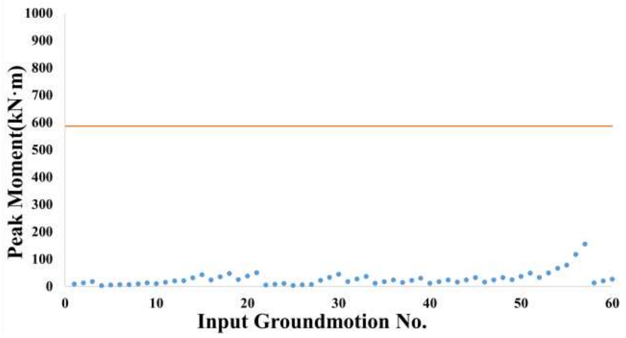

(a) Case-1 (Hard rock)

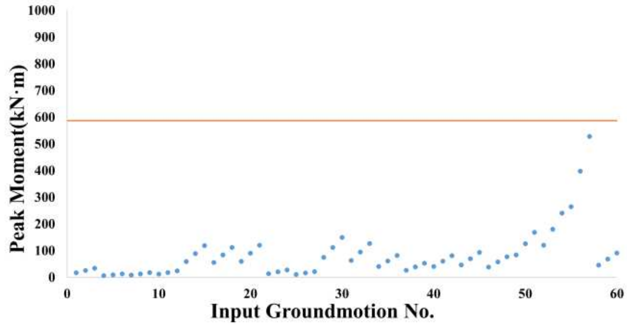

(b) Case-2 (Soft rock)

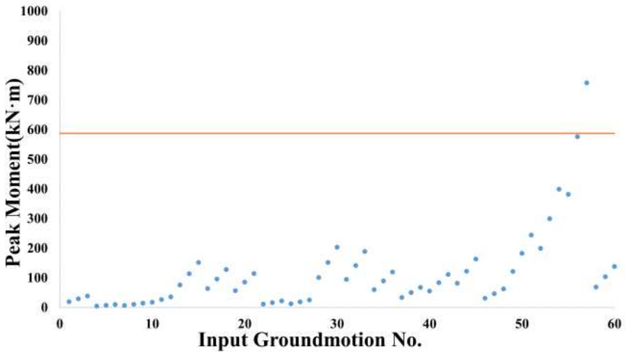

(c) Case-3 (Weathered rock)

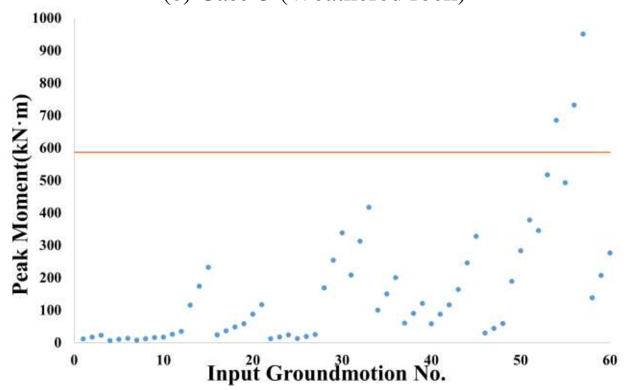

(d) Case-4 (Fault zone)

Figure 5. Peak Moment Responses Across All Seismic Inputs and Cases

Figure 5. Peak Moment Responses Across All Seismic Inputs and Cases

This indicates that the structural safety of the tunnel lining is progressively degraded as the ground stiffness decreases. Consequently, these weak ground sections can critically weaken the seismic performance of the tunnel, necessitating prioritized engineering attention and more rigorous evaluations during both the design and construction phases.

4 CONCLUSIONS

This study developed a dynamic numerical model to quantitatively evaluate the seismic response and structural safety of excavated tunnels under various rock and seismic conditions. A two-dimensional dynamic analysis model was constructed using OpenSees, in which domestic rock conditions were classified into four categories from hard rock (Case 1) to fault zone (Case 4). A total of 20 recorded domestic and international ground motions were scaled to three intensity levels to investigate the effects of rock stiffness and seismic intensity on the bending moment response of the tunnel lining.

The analysis results revealed that ground acceleration amplification was negligible for competent rock conditions, whereas the fault zone condition (Case 4), which exhibited the highest impedance contrast with the bedrock, showed a slight amplification of acceleration. The bending moment distribution along the horseshoe-shaped tunnel lining indicated that the sidewall–invert junction experienced the largest bending moment due to geometric discontinuity, suggesting that this region represents the most structurally vulnerable section under seismic loading.

Rock stiffness was found to play a dominant role in controlling both the moment response and seismic stability of the tunnel. As rock stiffness decreased, both static and dynamic bending moments increased due to enhanced soil–structure interaction and load redistribution. When the maximum bending moments obtained from 60 ground motion analyses were compared with the allowable flexural strength of 587 kN·m, most cases from hard to weathered rock (Cases 1–3) satisfied the structural safety criterion. However, under the fault zone condition (Case 4), three ground motions exceeded the allowable limit, demonstrating a significant increase in seismic fragility compared with sound rock conditions.

These findings challenge the conventional assumption that rock tunnels are inherently safe against earthquakes, highlighting that poor geological conditions such as fault zones can critically degrade their seismic performance. Therefore, detailed geotechnical investigations and site-specific seismic assessments should be prioritized in such zones, and future studies should focus on developing seismic fragility models to quantify the damage probability of tunnels under varying seismic intensity levels.

ACKNOWLEDGEMENTS

The authors are grateful for the financial support provided by the Korea Agency for Infrastructure Technology Advancement (KAIA). The project presented in this paper is supported by the Ministry of Land, Infrastructure and Transport under Grant No. RS-2023-00238458.

REFERENCES

Argyroudis, S. A., & Pitilakis, K. (2012). Seismic fragility curves of shallow tunnels in alluvial deposits. Soil Dynamics and Earthquake Engineering, 43, 1-15.

Bieniawski, Z. T. (1989). Engineering rock mass classifications: A complete manual for engineers and geologists in mining, civil, and petroleum engineering. John Wiley & Sons.

Drucker, D. C., & Prager, W. (1952). Soil mechanics and plastic analysis or limit design. Quarterly of Applied Mathematics, 10(2), 157-165.

Fajfar, P. (2000). A nonlinear analysis method for performance-based seismic design. Earthquake Engineering & Structural Dynamics, 29(12), 1771-1793.

Hashash, Y. M. A., Hook, J. J., Schmidt, B., & Yao, J. I. C. (2001). Seismic design and analysis of underground structures. Tunnelling and Underground Space Technology, 16(4), 247-293.

Hoek, E., & Brown, E. T. (1980). Underground excavations in rock. Institution of Mining and Metallurgy.

Hoek, E., Carranza-Torres, C., & Corkum, B. (2002). Hoek-Brown failure criterion: 2002 edition. Proceedings of the NARMS-TAC Conference, 1, 267-273.

Kappos, A. J., Panagopoulos, G., Panagis, C., & Penelis, G. G. (2006). A hybrid method for the vulnerability assessment of R/C and URM buildings. Bulletin of Earthquake Engineering, 4(4), 391-413.

Kramer, S. L. (1996). Geotechnical earthquake engineering. Prentice Hall.

Kuhlemeyer, R. L., & Lysmer, J. (1973). Finite element method accuracy for wave propagation. Journal of the Soil Mechanics and Foundations Division (ASCE), 99(5), 421-427.

Kwon, S. Y., Yoo, M., & Hong, S. (2020). Earthquake risk assessment of underground railway station by fragility analysis based on numerical simulation. Geomechanics and Engineering, 21(2), 143-152.

Ministry of Land, Infrastructure and Transport (MOLIT). (2021). KDS 14 20 00: 2021 Design standard for concrete structures. Sejong, Republic of Korea.

Ministry of Land, Infrastructure and Transport (MOLIT). (2021). KDS 47 10 40: 2021 Design standard for railway tunnels. Sejong, Republic of Korea.

O'Rourke, M. J., & Liu, X. (1999). Response of buried pipelines subjected to earthquake effects (MCEER-99-MN03). Multidisciplinary Center for Earthquake Engineering Research.

Wang, J. N. (1993). Seismic design of tunnels: A state-of-the-art approach. Parsons Brinckerhoff.